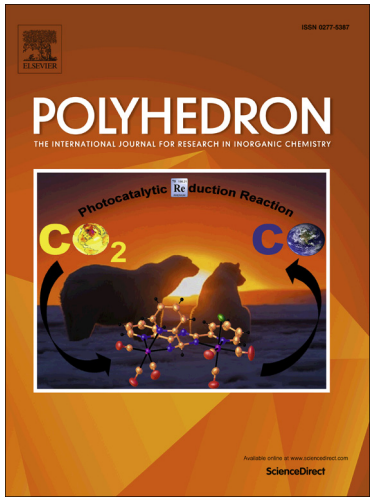

Synthesis, Characterization and Biological Activity of Gallium(III) Complexes with non-symmetrical N_2O-Donor Schiff Bases

Diego S. Padilha, Yan F. Santos, Letícia C. Giacomin, Frederico A.V. Castro, Marcos D. Pereira, Alexandre B. Rocha, Jackson A.L.C. Resende, Marciela Scarpellini

PII: S0277-5387(16)30671-4
DOI: http://dx.doi.org/10.1016/j.poly.2016.12.020
Reference: POLY 12378

To appear in: *Polyhedron*

Received Date: 20 September 2016
Revised Date: 12 December 2016
Accepted Date: 16 December 2016

Please cite this article as: D.S. Padilha, Y.F. Santos, L.C. Giacomin, F. A.V. Castro, M.D. Pereira, A.B. Rocha, J. A.L.C. Resende, M. Scarpellini, Synthesis, Characterization and Biological Activity of Gallium(III) Complexes with non-symmetrical N_2O-Donor Schiff Bases, *Polyhedron* (2016), doi: http://dx.doi.org/10.1016/j.poly.2016.12.020

Synthesis, Characterization and Biological Activity of Gallium(III) Complexes with non-symmetrical N_2O-Donor Schiff Bases

*Diego S. Padilha[a], Yan F. Santos[a], Letícia C. Giacomin[a], Frederico A. V. Castro[a], Marcos D. Pereira[a], Alexandre B. Rocha[a], Jackson A. L. C. Resende,[b,c] and Marciela Scarpellini[a]**

[a] Instituto de Química, Universidade Federal do Rio de Janeiro, 21945-970 Rio de Janeiro, RJ, Brazil

[b] Instituto de Química, Universidade Federal Fluminense, 24020–150, Niterói, RJ, Brazil

[c] Instituto de Ciências Exatas e da Terra, Centro Universitário do Araguaia, Universidade Federal do Mato Grosso, 786000-000 , Barra do Garças, MT, Brasil

*Corresponding Author: phon.: +55 21 3938 7742; fax: +55 21 3938 7559

e-mail address: marciela@iq.ufrj.br

Abstract

Cisplatin and its analogues are some of the most widely used anticancer drugs. However, toxicity and resistance have limited their use, and gallium compounds have emerged as an alternative, due to their remarkable antitumor activity and low toxicity. In this paper, we report four new mononuclear gallium(III) complexes with the general formula **[Ga(bhi-R)$_2$]$^+$**, where **bhi-R** (**R** = **–NO$_2$, –Br, –Cl** and **–OCH$_3$**) is the deprotonated form of imidazole/phenol-containing tridentate Schiff bases. The molecular structures of **C1**–**C4** were solved by single crystal X-ray diffraction revealing mononuclear and isostructural complexes, with the metal center in distorted octahedral geometries. In all cases, the gallium(III) is coordinated to two ligand molecules arranged in *meridional* fashion, through the imidazole and imino nitrogen atoms, and to the phenolate oxygen atom. Complexes **C1**–**C4** were also characterized in solution by spectroscopic and spectrometric techniques. DFT calculations were performed to assist the interpretation of experimental results, and also allowed to establish the reasons why only *meridional* isomers were obtained. The stability of all complexes was evaluated in PBS buffer (1% DMSO) over 24h, and results indicate partial hydrolysis in this period. Finally, the biological activity of **C1–C4** was evaluated on human tumor cell lines MCF-7 (breast adenocarcinoma), A-549 (lung adenocarcinoma epithelial) and PC-3 (prostate adenocarcinoma). Complex **C1** was the most active, being effective and selective for A-549. The IC_{50} (94.12 ± 4.62) of **C1** is lower than the value (135.10 ± 6.50) obtained for cisplatin, which was tested as a metallodrug reference under the same experimental conditions.

Keywords: Gallium complex, metallodrug, DFT calculation, X-ray crystal structure, tumor cell, MCF-7, A-549, PC-3 .

1. Introduction

Platinum-based anticancer agents have been successfully used in the clinic for the last 30 years. However, undesirable nephrotoxicity and resistance remain a challenge [1, 2]. In attempt to overcome these drawbacks, many researchers have focused on the development of cytotoxic compounds with improved properties using several metals [3, 4]. Among them, gallium has proved to be effective against some malignancies, even in the form of simple salts [5, 6].

The remarkable activity of gallium salts is contrasted by its reduced oral bioavailability, which was the main obstacle for the development of an oral formulation, along with renal toxicity [6, 7]. This adverse feature of gallium salts has led to the design of ligands capable to stabilize the gallium ion and prevent hydrolysis reactions [8, 9]. Some gallium complexes are now in advanced development stage, including gallium maltolate (Figure 1a) and KP46 (Figure 1b) [10, 11]. These complexes were designed to present improved oral bioavailability and have overcome phases I and II clinical trials with promising outcomes, encouraging researches on other classes of gallium complexes [12].

Recent work on the cytotoxic activity of gallium complexes of different *N,N,N*–, *N,N,O*– and *N,O,O*–donor ligands includes pyridine [13, 14] and pyrazole [15] Schiff bases, semicarbazones [16], hydrazones [17], and thiosemicarbazones [18, 19].

Expanding the number of gallium compounds with antitumor activity is a key step to achieve better understanding of the relevant properties involved in their biological activity, and thus contribute to the knowledge necessary for an effective drug design.

In this work, we report on four new gallium(III) complexes (Figure 1 c) of non-symmetrical *N,N,O*–donor Schiff base tridentate ligands, and their activities on the human tumor cell lines MCF-7 (breast adenocarcinoma), A-549 (lung adenocarcinoma) and PC-3 (prostate adenocarcinoma). Furthermore, in order to understand the reasons why only the *meridional* (*mer*) isomers were isolated, DFT/B3LYP calculations were employed to optimize the geometries of *meridional* (*mer*) and *facial* (*fac*) isomers for all complexes. DFT calculations were also carried out as an auxiliary tool to understand structural and electronic properties of complexes **C1**–**C4**.

2. Experimental section

2.1. General procedures

Ligands **HL1**–**HL4** were obtained by modifications on previously described methods for **HL1** [20]. To the best of our knowledge, **HL2-HL4** are unprecedented. All other chemicals were analytical grade and used for syntheses and analyses as received from commercial sources. The analyses of **C1**–**C4** were performed using only single crystalline samples. Infrared spectra of ligands and complexes were recorded in the range of 4000 to 400 cm^{-1}, in KBr pellets (or thin films) on a Nicolet Magna FTIR-760, or in a Shimadzu IRAffinity-1 spectrophotometer. Elemental analyses were obtained in a Thermo Scientific FlashEA 1112 CHNS/O Elemental Analyzer. Molar conductivity

measurements were performed on a Bel Engineering BE510 conductivimeter. Electronic spectra were recorded using a Varian Cary 50-Bio spectrophotometer, in methanol. Reactivity of **C1**–**C4** in PBS buffer pH 7.4 (1% DMSO) was evaluated by electronic spectroscopy, over 24h, in the same equipment described above. Cyclic voltammetry experiments were performed on a BAS Epsilon potentiostat, at room temperature (25 °C), in anhydrous DMF and under argon atmosphere. A standard three-electrode cell consisting of glass carbon working electrode, platinum wire auxiliary electrode and Ag/AgCl pseudo-reference electrode were employed. $LiClO_4$ [0,1 M] was used as supporting electrolyte and the ferrocenium-ferrocene couple [21] was employed as standard reference. Electrospray ionization-mass spectrometry (ESI-MS) of complexes **C1–C4** was carried out with a Perkin Elmer Flexar SQ 300 MS, in the positive mode, in methanol. ^{1}H (200, 300 or 500 MHz) and ^{13}C (50, 75 or 125 MHz) NMR spectra were obtained on a Bruker-DTX 200 MHz, or on a Bruker DRX 300MHz spectrophotometer in DMSO-d_6 solutions and referenced to TMS (tetramethylsilane). ^{1}H-^{1}H COSY experiments were also performed for complexes **C1**–**C4** (Figures S1-S4).

2.2. Synthesis of HL1–HL4

Ligands **HL1**–**HL4** were synthesized by Schiff condensation of equimolar amounts of the appropriate *para*-substituted aldehyde with histamine, using the same general procedure. To a methanolic solution of histamine cooled over ice bath, a methanolic solution of the aldehyde was added dropwise, under continuous stirring. After addition, the reaction mixture was stirred over ice bath for another 3 hours, when the solvent was removed under reduced pressure.

2-((2-(1H-imidazol-4-yl)ethylimino)methyl)-4-nitrophenol (**Hbhi-NO_2, HL1)**

Starting from 0.844 g (5 mmol) of 5-nitrosalicylaldehyde, 0.926 g of **HL1** were obtained as a yellow powder. Yield: 71%. FTIR (KBr, cm^{-1}): ($NH_{imidazole}$), 3430; ν(C-$H_{Ar/Alif}$), 3146-2849; ν(C=N_{imine}), 1643; ν(C=N)/(C=C), 1613-1450; (NO_{2assim}), 1328; ν(NO_{2sim}), 1254; ν(C-O), 1052; δ(CH_{Ar}), 890/830. ^{1}H NMR (DMSO-d_6, 200 MHz): δ 8.67 (s, 1H), 8.38 (d, J = 3.0 Hz, 1H), 8.03 (dd, J = 9.7, 3.1 Hz, 1H), 7.79 (d, J = 1.0 Hz, 1H), 6.97 (d, 1H), 6.61 (d, J = 9.7 Hz, 1H), 3.94 (t, J = 6.6 Hz, 3H), 2.97 (t, J = 6.5 Hz, 3H).

2-((2-(1H-imidazol-4-yl)ethylimino)methyl)-4-bromophenol (**Hbhi-Br, HL2)**

Starting from 1.005 g (5 mmol) of 5-bromosalicylaldehyde, 1.104 g of **HL2** were obtained as a yellow powder. Yield: 75%. FTIR (KBr, cm^{-1}): ($NH_{imidazole}$), 3432; ν(C-$H_{Ar/Alif}$), 3084-2867; ν(C=N_{imine}), 1629; ν(C=N)/(C=C), 1573-1478; δ(O-H_{phenol}), 1384; ν(C-O), 1049; ν(C-Br), 1046; δ(CH_{Ar}), 900/824. ^{1}H NMR (DMSO-d_6, 200 MHz): δ 8.49 (s, 1H), 7.80 (s, 1H), 7.63 (d, J = 2.5 Hz, 1H), 7.44 (dd, J = 8.8, 2.6 Hz, 1H), 6.91 (s, 1H), 6.83 (d, J = 8.8 Hz, 1H), 3.85 (t, J = 6.7 Hz, 2H), 2.90 (t, J = 6.9 Hz, 2H).

2-((2-(1H-imidazol-4-yl)ethylimino)methyl)-4-chlorophenol (**Hbhi-Cl, HL3)**

Starting from 1.278 g (8 mmol) of 5-methoxysalicylaldehyde, 1.978 g of **HL3** were obtained as a light-brown oil. Yield: 99%. FTIR (KBr, cm^{-1}): ν(C-$H_{Ar/Alif}$), 3094-2836; ν(C=N_{imine}), 1638; ν(C=N)/(C=C), 1574-1480; δ(CH_{Ar}), 874/822; δ(O-H_{phenol}), 1372; ν(C-O), 1028; ν(C-Cl), 1091. ^{1}H NMR (300 MHz, DMSO) δ 10.23 (s, 1H), 8.48 (s, 1H), 7.80 (s, 1H), 7.51 (d, J = 2.7 Hz, 1H), 7.33

(dd, *J* = 8.8, 2.7 Hz, 1H), 6.91 (s, 1H), 6.87 (d, *J* = 8.8 Hz, 1H), 3.84 (t, *J* = 6.8 Hz, 2H), 2.89 (t, *J* = 6.9 Hz, 2H).

2-((2-(1H-imidazol-4-yl)ethylimino)methyl)-4-methoxyphenol (**Hbhi-OCH_3, HL4)**

Starting from 0.7802 g (5 mmol) of 5-methoxysalicylaldehyde, 0.9865 g of **HL4** were obtained as a yellow-brown oil. Yield: 80%. FTIR (KBr, cm^{-1}): ν(C-$H_{Ar/Alif}$), 3137-2836; ν(C=N_{imine}), 1645; ν(C=N)/(C=C), 1592-1433; δ(O-H_{phenol}), 1392; ν(C-O-C_{ether}), 1272; ν(C-O), 1035; δ(CH_{Ar}), 870/822. ^{1}H NMR (DMSO-d_6, 200 MHz): δ 10.25 (s, 1H), 8.46 (s, 1H), 7.74 (s, 1H), 7.21 – 6.66 (m, 4H), 5.83 (s, 1H), 3.83 (t, *J* = 6.9 Hz, 2H), 3.70 (s, 3H), 2.88 (t, *J* = 7.0 Hz, 2H).

2.3 Synthesis of C1–C4

mer-[Ga(bhi-$NO_2)_2$]NO_3, **C1**. Complex **C1** was obtained by slow addition of $Ga(NO_3)_3$•$6H_2O$ (1 mmol in 30 mL of methanol) to a solution of **Hbhi-NO_2** (2 mmol in 30 mL of methanol). The reaction mixture was stirred for 2 hours, when the complex started to precipitate as a pale-yellow amorphous solid. This solid was filtered off and washed with cold isopropanol and diethyl ether. Yellow single crystals suitable for X-ray analysis were obtained by recrystallization in methanol:acetonitrile (1:1). Yield after recrystallization: 103 mg, 16%. MP: >310 ºC. FTIR (KBr, cm^{-1}): ($NH_{imidazole}$), 3389; ν(C-$H_{Ar/Alif}$), 3158-2930; ν(C=N_{imine}), 1629; ν(C=N)/(C=C), 1559-1430; (NO_{2assim}), 1318 (NO_{2sim}), 1270; ν(C-O) 1037; δ(CH_{Ar}), 878/832; δ(N-$O_{nitrate}$), 833. Elemental analysis (calc. for $C_{24}H_{22}GaN_9O_9$, FW: 650.21 g mol^{-1}) calc. (found): C, 44.3 (43.8); H, 3.40 (3.50); N, 19.4 (19.2) %. ESI-MS (CH_3OH): m/z^+ = 587,2070 (100%, [Ga(bhi-$NO_2)_2$]$^+$, $C_{24}H_{22}GaN_8O_6^+$,

m/z^+_{calc} = 587,0918). Λ_M = 14.7 Ω^{-1} mol^{-1} cm^2 (1:1 electrolyte in DMSO) [22]. ^{1}H NMR (DMSO-d_6, 200 MHz): δ 12.96 (s, 1H), 8.89 (s, 1H), 8.42 (d, J = 3.0 Hz, 1H), 8.09 – 7.93 (m, 2H), 7.11 (s, 1H), 6.58 (d, J = 9.3 Hz, 1H), 4.19 (dt, J = 25.9, 12.0, 7.7 Hz, 2H), 3.10 (t, J = 9.8 Hz, 2H). ^{13}C NMR (50 MHz, DMSO-d_6) δ 172.02, 171.64, 136.02, 135.78, 135.64, 132.36, 129.51, 122.20, 116.56, 114.47, 60.21, 24.58 (Figure S5).

mer-$[Ga(bhi\text{-}Br)_2]ClO_4 \bullet {}^3/_2H_2O \bullet {}^1/_2CH_3OH$, **C2**. Complex **C2** was synthesized by the slow addition of $Ga(NO_3)_3 \bullet 6H_2O$ (1 mmol in 30 mL of ethanol) to a solution of **Hbhi-Br** (2 mmol in 30 mL of ethanol), followed by the addition of KOH (2 mmol in 20 mL of ethanol). After 3 hours under stirring, an excess of $NaClO_4$ was added to the reaction mixture. The resulting solution was filtered to remove KNO_3. Yellow single crystals suitable for X-ray analysis were obtained from the mother liquor by slow evaporation at 15 ºC, after 2 days. Yield after recrystallization: 90 mg, 12%. MP: 255 (±3) ºC. FTIR (KBr, cm^{-1}): ($NH_{imidazole}$), 3390; ν(C-$H_{Ar/Alif}$), 3154-2934; ν(C=N_{imine}), 1629; ν(C=N)/(C=C), 1591-1466; (Cl-O), 1100; ν(C-O) 1032; δ(CH_{Ar}), 880/827. Elemental analysis (calc. for $C_{25}H_{28}Br_2ClGaN_6O_8$; FW: 805.51 g mol^{-1}) calc. (found): C, 37.3 (36.7); H, 3.50 (3.50); N, 10.4 (10.4) %. ESI-MS (CH_3OH): m/z^+ = 654,9680 (100%, $[Ga(bhi\text{-}Br_2)_2]^+$, $C_{24}H_{22}Br_2GaN_4O_2^+$, m/z^+_{calc} = 654,9401). Λ_M = 75.2 Ω^{-1} mol^{-1} cm^2 (1:1 electrolyte in methanol) [22]. ^{1}H NMR (DMSO-d_6, 200 MHz): δ 12.71 (s, 1H), 8.56 (s, 1H), 7.81 (s, 1H), 7.44 (d, J = 2.8 Hz, 1H), 7.22 (dd, J = 9.0, 2.7 Hz, 1H), 7.02 (s, 1H), 6.39 (d, J = 8.9 Hz, 1H), 4.09 (dt, J = 34.0, 11.6, 8.2 Hz, 2H), 3.04 (dt, J = 24.3, 9.3, 5.3 Hz, 2H). ^{13}C NMR (50 MHz, DMSO-d_6) δ

170.85, 165.88, 137.08, 136.18, 135.29, 123.66, 119.19, 114.01, 104.61, 59.84, 24.79, 18.54 (Figure S6).

mer-[Ga(bhi-Cl)$_2$]ClO$_4$•CH$_3$OH, **C3**. Complex **C3** was obtained by slow addition of Ga(NO$_3$)$_3$•6H$_2$O (1 mmol in 30 mL of methanol) to a methanol solution of ligand **Hbhi-Cl** (2 mmol), followed by the addition of KOH (2 mmol in 20 mL of ethanol). The reaction mixture was stirred for 16 hours and then an excess of NaClO$_4$ was added. Precipitated KNO$_3$ was removed by filtration. Yellow single crystals suitable for X-ray analysis were obtained by slow evaporation of the mother liquor after 2 days, at 15 ºC. Yield after recrystallization: 360 mg, 32%. MP: 238 (±3) ºC. FTIR (KBr, cm^{-1}): ν(C-H$_{Ar/Alif}$), 3151-2936; ν(C=N$_{imine}$), 1630; ν(C=N)/(C=C), 1595-1466; (Cl-O), 1099; ν(C-O), 1030; δ(CH$_{Ar}$), 875/827. Elemental analysis (calc. for C$_{24}$H$_{28}$Cl$_3$GaN$_6$O$_9$; FW: 720.60 g mol^{-1}) calc. (found): C, 40.0 (40.2); H, 3.92 (3.90); N, 11.66 (11.8) %. ESI-MS (CH$_3$OH): *m/z*$^+$ = 567,1660 (100%, [Ga(bhi-Cl)$_2$]$^+$, C$_{24}$H$_{22}$Cl$_2$GaN$_6$O$_2^+$, *m/z*$^+_{calc}$ = 567.0995), Λ_M = 76,1 Ω^{-1} mol^{-1} cm^2 (1:1 electrolyte in methanol) [22]. ^{1}H NMR (DMSO-*d*$_6$, 300 MHz): δ 12.72 (s, 1H), 8.57 (s, 1H), 7.82 (s, 1H), 7.32 (d, *J* = 2.8 Hz, 1H), 7.13 (dd, *J* = 9.0, 2.8 Hz, 1H), 7.02 (s, 1H), 6.44 (d, *J* = 9.0 Hz, 1H), 4.30 – 3.92 (m, 2H), 3.16 – 2.89 (m, 2H). ^{13}C NMR (125 MHz, DMSO-*d*$_6$) δ 171.44, 166.09, 136.72, 135.86, 135.01, 133.66, 123.77, 118.88, 118.07, 114.56, 60.39, 25.34 (Figure S7).

mer-[Ga(bhi-OCH$_3$)$_2$]ClO$_4$•H$_2$O•CH$_3$OH, **C4**. Complex **C4** was obtained by the same procedure described for **C3**. Green single crystals suitable for X-ray analysis were obtained by slow evaporation of the mother liquor after 1 day at

room temperature. Yield after recrystallization: 338 mg, 48%. MP: 244 (±3) ºC. FTIR (KBr, cm^{-1}): ν(C-$H_{Ar/Alif}$), 3150-2953; ν(C=N_{imine}), 1632; ν(C=N)/(C=C), 1584-1437; ν(C-O-C_{ether}), 1266; (Cl-O), 1092 ν(C-O), 1025; δ(CH_{Ar}), 866/811. Elemental analysis (calc. for $C_{27}H_{34}ClGaN_6O_{10}$; FW: 707.77 g mol^{-1}) calc. (found): C, 45.8 (44.3); H, 4.8 (4.9); N, 11.8 (11.7) %. ESI-MS: m/z^+ = 557,1000 (100%, $[Ga(bhi\text{-}OCH_3)_2]^+$, $C_{26}H_{28}GaN_6O_4^+$, m/z^+_{calc} = 557,1423). Λ_M = 77.9 Ω^{-1} mol^{-1} cm^2 (1:1 electrolyte in methanol) [22]. ^{1}H NMR (DMSO-d_6, 200 MHz): δ 12.61 (s, 1H), 8.55 (s, 1H), 7.75 (s, 1H), 7.00 (s, 1H), 6.90 – 6.71 (m, 2H), 6.40 (d, J = 9.0 Hz, 1H), 4.12 (dt, J = 42.6, 11.7, 11.7 Hz, 2H), 3·64 (s, 3H), 3.15 – 2.87 (m, 2H). ^{13}C NMR (50 MHz, DMSO-d_6) δ 171.18, 161.93, 148.48, 136.34, 135.06, 123.87, 122.07, 116.30, 115.75, 113.69, 59.66, 55.47, 48.59, 24.97 (Figure S8).

2.3. X-ray crystallography

Suitable single crystals for X-ray diffraction experiments of **C1** were obtained by recrystallization in methanol:acetonitrile (1:1) solution. For complexes **C2**–**C4**, crystals were obtained by slow evaporation of mother liquors. Selected crystals of **C1**, **C2** and **C4** were analyzed on a Bruker Nonius Kappa CCD diffractometer using MoKα radiation (λ = 0.71073) at room temperature. The data collection was performed using *Collect* [23] and reduced using *EvallCCD* software [24]. For complex **C3**, the data acquisition was performed in a Bruker D8 Venture diffractometer with MoKα radiation, at room temperature. The *ApexII* software [25] was used in the processing and data reduction. Structures were solved by direct methods using *SHELXS-13* software [26]. All non-hydrogen atoms were refined anisotropically on F^2 by the full-

matrix least-square technique using *SHELXL-13* software [26]. Hydrogen atoms were generated geometrically and treated by a mixture of independent and constrained refinement.

2.4. *In vitro* biological assays

The human cancer cell lines A-549, MCF-7, and PC-3, were cultured in DMEM supplemented with 10% fetal bovine serum (FBS), 2 mmol/L of L-glutamine, 100 U/mL of penicillin and 100 µg/mL of streptomycin (Invitrogen, Carlsbad, CA, USA), at 37 °C, and 5% CO_2 humidified atmosphere. Complexes **C1**–**C4** were initially dissolved in DMSO at a final concentration of 50 mmol/L, and then further diluted directly in DMEM prior the tests. In addition, final DMSO concentration did not exceed 1% during cytotoxic tests. For determination of **C1**–**C4** toxicity, 1.25×10^4 cells/mL were seeded in quadruplicate into 96-well plates and incubated at 37 °C, in a 5% CO_2 humidified atmosphere (Tecnal, TE-399). The culture medium was replaced by a freshly prepared DMEM medium containing increasing concentration of **C1**–**C4** (10, 25, 50, 75, 100, 150 and 200 µmol/L), and incubated as described above. After 24 h, cells were washed and 0.100 mL of a 0.5 mg/mL solution of [3-(4,5-dimethylthiazol-2-yl)-2,5-diphenyltetrazolium bromide] (MTT) in DMEM FBS-free was added. Then, the plates were incubated for 3 h with MTT and after this period, the solution was removed and formazan crystals were solubilized with 0.1 mL/ well DMSO. Survival was analyzed spectrophotometrically at 570 nm using a *HT PowerWave* XS microplate reader (BioTeK). IC_{50} was calculated by a non-linear regression from log transformation of the dose-response curves. Data were obtained from three independent experiments [27].

2.5. DFT calculations

Complexes geometries were optimized with cc-pVDZ basis set and zero point corrections were performed in each case, at the equilibrium geometries. Since heavy atoms are present, the influence of relativistic effects was also studied at the equilibrium geometry by the Douglas-Kroll-Hess Hamiltonian corrected to third order [28, 29]. In the last case, a larger basis set cc-pVTZ-DK was used, which is more appropriated to this kind of calculation. All calculations were performed with GAMESS suite of programs.

3. Results and Discussion

3.1 Synthesis and Characterization

Ligands **HL1**–**HL4** were synthesized in desirable purity and yield by condensation reactions of the appropriate *para*-substituted salicylaldehyde with histamine, using modifications on previously reported methodology for **HL1** [20]. Ligands **HL1** and **HL2** were obtained as yellow powders, while **HL3** and **HL4** were isolated as light-brown and yellow-to-brown oils, respectively, which solidified after two days in desiccator. Complexes **C1**–**C4** were obtained in low to moderate yields by treating each ligand with $Ga(NO_3)_3 \cdot 6H_2O$ (2:1 molar ratio), in methanol or ethanol, in the presence of an auxiliary base (KOH). In the absence of KOH, the complexation reaction leads to a mixture of the desired complex and the nitrate salt of the protonated ligand. These species were characterized by X-ray single crystal crystallography and data are not shown here. This indicates that part of the ligand is acting as a base to deprotonate the phenol and assisting the complexation reaction.

Characterization of **C1**–**C4**, including single crystal X-ray diffraction, supports the obtaining of mononuclear and isostructural gallium(III) complexes, in pseudo-octahedral environments. The molecular ion peak $[Ga(bhi\text{-}R)_2]^+$ was observed on the mass spectrum of compounds **C1**–**C4**, in good agreement between experimental and calculated isotopic distribution patterns. Molar conductivity values for **C1**–**C4** are in the range found for 1:1 electrolytes [22], as expected for monocationic complexes. Compounds **C1**–**C4** are soluble in most of polar solvents, but **C1** is only slightly soluble in water and methanol.

3.2 Crystal structures and structural properties

Crystal structures of **C1**–**C4** were solved by single crystal X-ray diffraction. Crystallographic and refinement data are shown in Table 1. Thermal ellipsoid drawing for **C1** is presented in Figure 2, and in Figures S9 – S11 for **C2**–**C4**. Results for **C1**–**C4** show the gallium(III) center surrounded by two molecules of the respective ligand in a *meridional* pseudo-octahedral environment. Ligands coordinate to the metal center through the imidazole and the imine nitrogen atoms, and the phenolate oxygen, with an $[Ga<N_{imine1}N_{imine2}><N_{imidazole1}O_{phenol2}> <N_{imidazole2}O_{phenol1}>]$ arrangement [30, 31]. Complexes **C1** and **C2** crystallize in the monoclinic crystal system, belonging to the $P2_1/n$ space group. Complex **C4** is also in the monoclinic system, but in the *Cc* space group. Complex **C3** crystallizes in the orthorhombic crystal system, in *Pbca* space group. The asymmetric unit of **C1** is composed by one molecule of the cation complex $[Ga(bhi\text{-}NO_2)_2]^+$ and one nitrate molecule as counter ion. The nitrate forms hydrogen bonds with the N–H group of the imidazole ring (Figure 2) that are relevant to uphold the crystal lattice. For complex **C2**, the unit

cell shows the presence of two crystallographically independent $[Ga(bhi\text{-}Br)_2]^+$ molecules that are slightly different in bond distances and angles. Two perchlorate anions, three water and one methanol molecules are also observed. In the case of complexes **C3** and **C4** the structure exhibits a single molecule of the cation complex surrounded by one perchlorate and one methanol. For complex **C4,** a water molecule is also present. Complex **C3** shows a vibrational crystallographic disorder in the ethylene group of one of the **bhi-Cl** ligands and a rotational disorder in the perchlorate counter ion. Complexes **C1**–**C4** show comparable bond lengths and angles, with average distances of 1.940 Å for **Ga**–$\mathbf{O_{phenol}}$, 2.056 Å for **Ga**–$\mathbf{N_{imine}}$ and 2.074 Å for **Ga**–$\mathbf{N_{imidazole}}$. These values are in good agreement with similar gallium(III) complexes reported in the literature [13, 15, 31]. Correlations between the Hammett parameter of phenol ring substituents in *para* position (σ_p) and **Ga**–$\mathbf{N_{imine}}$ or **Ga**–$\mathbf{O_{phenol}}$ bond lengths were observed. For **Ga**–$\mathbf{N_{imine}}$, the increase in electron withdrawing effect (–$\mathbf{OCH_3}$ < –**Br** ≈ –**C**l < –$\mathbf{NO_2}$) leads to a decrease in the bond length, while the opposite effect is observed for **Ga**–$\mathbf{O_{phenol}}$ (Table 2). Shortening of **C**–**O** bond lengths was also observed. This trend can be illustrated by the decrease of p*K*a values for *para*-substituted phenols as the electron withdrawing effect increases. This effect was experimentally and theoretically observed before [32, 33], where good agreement between σ_p values and *pK*a was found.

As already mentioned, DFT calculations were carried out in order to understand the preference for the *meridional* coordination mode of the tridentate ligand observed here. *Meridional* (*mer*) and *facial* (*fac*) isomers of gallium(III) complexes with **HL1**–**HL4** were evaluated and the calculated relative energies are presented in Table 3. In all cases, the *mer* isomer is the most

stable. The relative energy values in column A are the difference of total energies calculated at equilibrium geometry. In column B, relative energies were calculated by the same procedure adopted in column A, but total energies were corrected for relativistic effects through the Douglas-Kroll-Hess Hamiltonian. In column C, relative energies were calculated by the same procedure, but total energies were corrected with zero point energy (ZPE), i.e. taking into account the vibrational ground state energy. Finally, in column D, both relativistic and ZPE corrections were considered. Differences in relative energies depend on the correction applied but, in all cases, these differences are higher than 30 Kcal/mol. This is a remarkable value and is higher than that found in other cases where *mer*/*fac* relative energies were calculated [31]. Figure S12 presents the final optimized structures of *mer* and *fac* isomers for **C1**. It can be observed that the *fac* isomer presents large steric constraints that enforce the break of one **Ga–N_{imine}** bond. It results in a less stable pentacoordinated species, whereas the *mer* isomer remains six coordinated. The absence of one chemical bond explains such a large difference in energy between the two isomers and may explain the reason why the *fac* isomer was not able to be isolated.

3.3 Spectroscopic and redox behavior

^{1}H NMR data for ligands and complexes are in good agreement with proposed structures. The presence of a single set of signals (Figure S13) is an indicative of the complexes stability in DMSO solution, since no sign of ligand release was observed. ^{1}H-^{1}H COSY (Figures S1–S4) experiments were carried out for complexes **C1**–**C4** and results were helpful to perform the assignments.

Comparing the data (Table S1) of free and complexed ligands, a downfield shift is observed for hydrogen atoms H5 and H7, indicating that there is coordination with nearby nitrogen atoms of the imidazole and imine groups in solution [34]. The same behavior is observed for H4, but less pronounced. On the other hand, an inverse behavior occurs for H3 and an upshift is detected for **C2-C4** and is almost null for **C1**. In general, the $–NO_2$ promotes a downshift of the ^{1}HNMR spectrum compared to the other substituents in this series of complexes. For –Br, –Cl and $–OCH_3$ no clear trends are observed for the chemical shifts of H4, H5, H7 and H8.

Electronic spectra of **HL1**–**HL4** (Figure S14) and complexes **C1**–**C4** (Figure 3) were recorded in methanol and Table 4 summarizes the data. A strong band around 400 nm is observed in the spectra of **HL1**–**HL4** and is blue-shifted in the spectra of **C1**–**C4**. This band can be attributed to $\pi \rightarrow \pi^*$ intraligand charge transfer transitions (ILCT) and, as its position is sensitive to the nature of phenol ring substituent, it might involve the imine moiety. In both, free and complexed compounds, this band undergoes a redshift as the electron withdrawing power of the substituent decreases. This band ranges from 350 nm for **C1** ($–NO_2$) to 370 nm, for **C2** (–Br) and **C3** (–Cl), and 390 nm for **C4** ($–OCH_3$). The same behavior is observed for the band around 265 nm that ranges from 250 nm for **C1** to 275 for **C4**. All the bands are attributed to intraligand charge transfer transition processes since the gallium(III) ion is a d^{10} system and do not present metal involved charge transfer transitions. Hyperchromic effect is observed for all bands after coordination.

Considering that redox processes are one of the modes of action of cytotoxic substances [35], cyclic voltammetry experiments were performed to

assess and compare the redox behavior of free and complexed ligands, since gallium(III) is well known to be redox inactive in biological systems. DMF was used as solvent due to its broader work window, when compared to methanol or water. Voltammograms were recorded in cathodic scans, at several scan rates, and in the potential range of +1.0 to -2.5 V using complexes concentration of 1.0 x 10^{-3} mol L^{-1}. Voltammograms of **C1**–**C4** are presented in Figure S15 and the data are summarized in Table 4. The CV of all ligands and complexes show an irreversible reduction process around -2.4 V *vs* Fc^{+}/Fc (Peak B). This process undergoes cathodic shift (more negative values) of about 0.1 V *vs* Fc^{+}/Fc after coordination, unless for **HL2** and **C2**. The similarities among the values suggest it should arise from the reduction of the imine. This group is common to all compounds and seems not to be affected by the substituents in the phenol ring. **HL1** and **C1** present an additional irreversible reduction around -1.9 V *vs* Fc^{+}/Fc (Peak A). It can be tentatively assigned to the one-electron reduction of $–NO_2$ to the nitro radical anion $NO_2^{\bullet -}$ [36]. Irreversible oxidation processes are observed for ligands and complexes. Peak C observed for **C2** in -0.9 V *vs* Fc^{+}/Fc (Figure S15) is tentatively attributed to the oxidation of the species containing the $NO_2^{\bullet -}$ group. In all complexes, peaks D and E are subtle to the substituent in the phenol ring, and should be related to the oxidation of the two phenol groups yielding phenoxyl radicals [37]. However, no correlation was found with the σ_p Hammet parameters and steric effects of the substituents can overcome the electronic ones.

3.4 Reactivity

Considering the strong tendency of gallium(III) complexes to hydrolyze in solution, **C1**–**C4** were spectroscopically monitored over 24h, in PBS buffer, pH 7.4, containing 1% DMSO, at 1.0×10^{-5} mol L^{-1}. At the region around 400 nm, a decrease in the absorption is observed for all complexes, as shown in Figure S16. Results can be rationalized in terms of Hammett parameter (σ_p) and hydrolysis. As σ_p increases, the tendency to undergo hydrolysis reactions reduces. For complex **C1** (σ_p = 0.78), a decrease of 17% in the absorption was observed, while 76% was found for complex **C4** (σ_p = -0.27). These results suggest that gallium(III) complexes with electron withdrawing ligands are prone to be more stable in the biological media, which could lead to higher biological activities. In addition, lower hydrolysis rates are desirable for application of gallium-based chemotherapeutics, which should be effective in short time exposure.

3.5 Biological activity

Human cancer cell lines (MCF-7, PC-3 and A-549) were exposed to increasing concentrations of ligands **HL1**–**HL4**, complexes **C1**–**C4** and $Ga(NO_3)_3 \cdot 6H_2O$ over 24 h. This time exposure was chosen taking into account the stability/hydrolysis data discussed above. The anticancer drug cisplatin was used as standard metallodrug in cytotoxic assays. After the time exposure, cell survival was evaluated and data are presented in Figure 4. At low concentrations, none of the ligands and complexes significantly affects cell survival, which only occurs above 150 μM. Thus, this value was taken as the

lower threshold for comparisons. For MCF-7 cell line (Figure 4A and D), at 150 μM, the anticancer activity of compounds follow the order **C4** < **C2** < **C3** < **C1** < **cisplatin**, and **$Ga(NO_3)_3$•$6H_2O$** < **HL1** < **HL2** ≈ **HL4** < **HL3**. Considering the PC-3 cell line (Figure 4B and E) at the same drug concentration, the order **C4** < **C3** ≈ **cisplatin** < **C2** < **C1**, and **$Ga(NO_3)_3$•$6H_2O$** < **HL3** < **HL1** ≈ **HL2** ≈ **HL4** is observed. Finally, in A-549 cell line (Figure 4C and F), the cytotoxic profile of tested compounds is **C2** < **C3** < **C4** < **cisplatin** < **C1**, and **HL1** ≈ **HL2** ≈ **HL4** < **$Ga(NO_3)_3$•$6H_2O$** < **HL3**. Then, considering data at 150 μM of cell exposure, **C1** is the most active complex against all lineages, showing cell survivals of 61.5 ± 2.1 % in MCF-7, 53.5 ± 3.5 % in PC-3 and 40.9 ± 0.5 % in A-549. For PC-3 and A-549 cell lines, **C1** proved to be even better than cisplatin, which displayed survival rates of 70.0 ± 4.5 and 46.5 ± 3.7 % for PC-3 and A-549, respectively. However, analyzing IC_{50} (Table 5), all tested compounds presented values higher than 200 μM for both MCF-7 and PC-3 cell lines. In the case of A-549, results point to an effectiveness and selectivity of **C1**, with lower IC_{50} (94.1 ± 4.6) than cisplatin (134.3 ± 7.6). When the activities of complexes are compared to that of the free ligands, a significant increase after coordination is observed only for **C1**, which presented an average decrease of 35% in survival rates. For **C2** – **C4** the difference is within the standard deviation.

The higher activity of **C1** compared to the other tested compounds might be related to the presence of the **–NO_2** substituent, which is known to undergo redox reactions in the biological media, generating cytotoxic products [38]. Other possible explanation for the enhanced activity of complex **C1** is its low solubility in polar solvents along with its lower tendency to undergo hydrolysis reactions, that might lead to a higher cell uptake of **C1** compared to the other

complexes. These IC_{50} values are higher than those reported for other gallium(III) complexes tested against the same cell lines, but differences in time incubation must be taken into account. Indeed, we believe that the activity strength of an antitumor drug is better evaluated during short exposure times, when it is expected to kill most of tumor cells. Gallium(III) complexes with semicarbazones ligands of salicylaldehyde derivatives [16] showed IC_{50} values between 23 and 164 μM after 72h of incubation. Values in the range of 13.3 to 52 μM were also observed after 72h for similar gallium(III) complexes with tridentate ligands pyrazol-imino-phenol type reported by Silva and coworkers [15].

4. Conclusions

In this work four new mononuclear and isostructural gallium(III) complexes with non-symmetric tridentade ligands were obtained. Complexes **C1**–**C4** show ligands coordinated in a meridional fashion, which was found to be the more thermodynamically favorable configuration, according to DFT calculations. The redox and electronic behavior of **C1**–**C4** are ligand-centered and does not involve the gallium(III) ion. The reduction of imine to amine is suggested to be the main observed redox process. Reduction of the NO_2 group was also observed and oxidation processes are tentatively attributed to the generation of phenoxyl radicals.

Complexes **C1**–**C4** proved not to be highly cytotoxic against the tested tumor lineages MCF-7 and PC-3. Complexes **C1** and **C4** were the most active compounds and capable to inhibit the A-549 cell growth in concentrations lower than 94.12 ± 4.62 μM and 174.70 ± 8.41 μM, respectively. Complexes **C1** and

C4 were active only against A-549 cell line, hence indicating a possible selectivity. In addition, **C1** is more active than the clinically standard metallodrug cisplatin (IC_{50} = 135.10 ± 6.5 μM) in the same experimental conditions. The nature of the phenol ring substituent was found to be relevant for the cytotoxic activity, however the mechanisms of action require further evaluation.

Future directions include the obtaining of novel gallium complexes containing the related amine ligands and the replacement of imidazole ring to pyridine in order to evaluate the effect of these modifications on the antitumor activity. These results are promising and can guide further research aiming at the development of gallium-based antitumor metallodrugs.

Appendix A. Supplementary data CCDC 1441117 - 1441120 contain the supplementary crystallographic data for **C1** - **C4**. These data can be obtained free of charge via http://www.ccdc.cam.ac.uk/conts/retrieving.html, or from the Cambridge Crystallographic Data Centre, 12 Union Road, Cambridge CB2 1EZ, UK; fax: (+44) 1223-336-033; or e-mail: deposit@ccdc.cam.ac.uk.

5. Acknowledgements

The authors are grateful to Professors Nicolás A. Rey and Ricardo Aucélio (PUC-RJ) for elemental analyses, Professor Mauricio Lanznaster (UFF) for ESI-MS analyses, and grants from Capes, CNPq (476269/2011-3) and Faperj (E-26/111.177/2011, E-26/110.157/2014) Financial Agencies.

6. References

[1] Graf, N., & Lippard, S. J. (2012). Redox activation of metal-based prodrugs as a strategy for drug delivery. *Advanced drug delivery reviews*, *64*(11), 993-1004. (**DOI:** 10.1016/j.addr.2012.01.007)

[2] Gianferrara, T., Bratsos, I., & Alessio, E. (2009). A categorization of metal anticancer compounds based on their mode of action. *Dalton Transactions*, (37), 7588-7598. (**DOI:** 10.1039/B905798F)

[3] Kaluderovic, G. N., & Paschke, R. (2011). Anticancer metallotherapeutics in preclinical development. *Current medicinal chemistry*, *18*(31), 4738-4752. (**DOI:** http://dx.doi.org/10.2174/092986711797535308)

[4] Komeda, S., & Casini, A. (2012). Next-generation anticancer metallodrugs. *Current topics in medicinal chemistry*, *12*(3), 219-235. (**DOI:** http://dx.doi.org/10.2174/156802612799078964)

[5] Bernstein, L. R. Therapeutic Gallium Compounds. In: Gielen, M., & Tiekink, E. R. (Eds.). (2005). *Metallotherapeutic drugs and metal-based diagnostic agents: the use of metals in medicine*. Padstow: John Wiley & Sons, 2005. p. 259-278. (**DOI:** 10.1002/0470864052.ch14)

[6] Chitambar, C. R. (2012). Gallium-containing anticancer compounds. *Future medicinal chemistry*, *4*(10), 1257-1272. (**DOI:** 10.4155/fmc.12.69)

[7] Dabrowiak, J. C. Metals in Medicine. Chippenham: John Wiley & Sons, 2009. p. 177-181. (**DOI:** 10.1002/9780470684986)

[8] Bratsos, I.; Gianferrara, T.; Alessio, E.; Hartinger, C. G.; Jakupec, M. A.; Keppler, B. K. Ruthenium and Other Non-platinum Anticancer Compounds. In: Alessio, E. (Ed.). (2011). *Bioinorganic medicinal chemistry*. Weinheim: Wiley-VHC, 2011. p. 151-174. (**DOI:** 10.1002/9783527633104.ch5)

[9] Lessa, J. A., Parrilha, G. L., & Beraldo, H. (2012). Gallium complexes as new promising metallodrug candidates. *Inorganica Chimica Acta*, *393*, 53-63. (**DOI:** 10.1016/j.ica.2012.06.003)

[10] Chitambar, C. R., Purpi, D. P., Woodliff, J., Yang, M., & Wereley, J. P. (2007). Development of gallium compounds for treatment of lymphoma: gallium maltolate, a novel hydroxypyrone gallium compound, induces apoptosis and circumvents lymphoma cell resistance to gallium nitrate. *Journal of Pharmacology and Experimental Therapeutics*, *322*(3), 1228-1236. (**DOI:** 10.1124/jpet.107.126342)

[11] Bonchi, C., Imperi, F., Minandri, F., Visca, P., & Frangipani, E. (2014). Repurposing of gallium-based drugs for antibacterial therapy. *Biofactors*,*40*(3), 303-312. (**DOI:** 10.1002/biof.1159)

[12] Enyedy, É. A., Dömötör, O., Bali, K., Hetényi, A., Tuccinardi, T., & Keppler, B. K. (2014). Interaction of the anticancer gallium (III) complexes of 8-hydroxyquinoline and maltol with human serum proteins. *JBIC Journal of Biological Inorganic Chemistry*, *20*(1), 77-88.
(**DOI:** 10.1007/s00775-014-1211-9)

[13] Shakya, R., Peng, F., Liu, J., Heeg, M. J., & Verani, C. N. (2006). Synthesis, structure, and anticancer activity of gallium (III) complexes with

asymmetric tridentate ligands: growth inhibition and apoptosis induction of cisplatin-resistant neuroblastoma cells. *Inorganic chemistry*, *45*(16), 6263-6268. (**DOI:** 10.1021/ic060106g)

[14] Chen, D., Frezza, M., Shakya, R., Cui, Q. C., Milacic, V., Verani, C. N., & Dou, Q. P. (2007). Inhibition of the proteasome activity by gallium (III) complexes contributes to their anti–prostate tumor effects. *Cancer research*,*67*(19), 9258-9265. (**DOI:** 10.1158/0008-5472.CAN-07-1813)

[15] Silva, F., Marques, F., Santos, I. C., Paulo, A., Rodrigues, A. S., Rueff, J., & Santos, I. (2010). Synthesis, characterization and cytotoxic activity of gallium (III) complexes anchored by tridentate pyrazole-based ligands.*Journal of inorganic biochemistry*, *104*(5), 523-532. (**DOI:** 10.1016/j.jinorgbio.2010.01.003**)**

[16] Gambino, D.; Fernández, M.; Santos, D.; Etcheverría, G. A.; Piro, O. E.; Pavan, F. R.; Leite, C. Q. F.; Tomaz, I.; Marques, F. (2011). Searching for gallium bioactive compounds: Gallium (III) complexes of tridentate salicylaldehyde semicarbazone derivatives. *Polyhedron*, *30*(7), 1360-1366. (**DOI:** 10.1016/j.poly.2011.02.037)

[17] Machado, I.; Fernández, M.; Becco, L.; Garat, B.; Brissos, R.F. ; Zabarska, N.; Gamez, P.; Marques, F.; Correia, I.; Costa Pessoa, J.; Gambino, D. (2014). New metal complexes of NNO tridentate ligands: Effect of metal center and co-ligand on biological activity. *Inorganica Chimica Acta*, *420*, 39-46. (**DOI:** 10.1016/j.ica.2013.10.022)

[18] Kumar, K.; Schniper, S.; Gonzalez-Sarrías, A.; Holder, A. A.; Sanders, N.; Sullivan, D.; Jarrett, W. L.; Davis, K.; Bai, F.; Seeram, N. P.; Kumar, V. (2014).

Highly potent anti-proliferative effects of a gallium (III) complex with 7-chloroquinoline thiosemicarbazone as a ligand: Synthesis, cytotoxic and antimalarial evaluation. *European journal of medicinal chemistry*, *86*, 81-86. (**DOI:** 10.1016/j.ejmech.2014.08.054)

[19] Parrilha, G. L.; Ferraz, K. S. O.; Lessa, J. A.; Oliveira, K. N.; Rodrigues, B. L.; Ramos, J. P.; Souza-Fagundes, E. M.; Ott, I.; Beraldo, H. (2014). Metal complexes with 2-acetylpyridine-N (4)-orthochlorophenylthiosemicarbazone: Cytotoxicity and effect on the enzymatic activity of thioredoxin reductase and glutathione reductase. *European journal of medicinal chemistry*, *84*, 537-544. **(DOI:** 10.1016/j.ejmech.2014.07.055)

[20] Baldwin, M. J., Kampf, J. W., Kirk, M. L., & Pecoraro, V. L. (1995). Structural and Magnetic Studies of Manganese (II) Complexes of the Imidazole-Containing Ligand 5-NO2-salimH [5-NO2-salimH2= 4-(2-((5-nitrosalicylidene) amino) ethyl) imidazole] with Varying Nuclearity. *Inorganic Chemistry*, *34*(21), 5252-5260. (**DOI:** 10.1021/ic00125a026)

[21] Gagne, R. R., Koval, C. A., & Lisensky, G. C. (1980). Ferrocene as an internal standard for electrochemical measurements. *Inorganic Chemistry*,*19*(9), 2854-2855. (**DOI:** 10.1021/ic50211a080)

[22] Geary, W. J. (1971). The use of conductivity measurements in organic solvents for the characterisation of coordination compounds. *Coordination Chemistry Reviews*, *7*(1), 81-122. (**DOI:** 10.1016/S0010-8545(00)80009-0)

[23] Bruker (2008). COLLECT. Bruker AXS Inc., Madison, Wisconsin, USA.

[24] Duisenberg, A. J., Kroon-Batenburg, L. M., & Schreurs, A. M. (2003). An intensity evaluation method: EVAL-14. *Journal of applied crystallography*,*36*(2), 220-229. (**DOI:** 10.1107/S0021889802022628)

[25] Bruker (2014). *ApexII*. Bruker AXS Inc., Madison, Wisconsin, USA.

[26] Sheldrick, G. M. (2007). A short history of SHELX. *Acta Crystallographica Section A: Foundations of Crystallography*, *64*(1), 112-122. (**DOI:** doi:10.1107/S0108767307043930)

[27] Freshney, R. (2005). Culture of animal cells: A manual of basic technique (5th ed.). Hoboken, N.J.: Wiley-Liss.

[28] Douglas, M., & Kroll, N. M. (1974). Quantum electrodynamical corrections to the fine structure of helium. *Annals of Physics*, *82*(1), 89-155. (**DOI:** 10.1016/0003-4916(74)90333-9)

[29] Hess, B. A. (1986). Relativistic electronic-structure calculations employing a two-component no-pair formalism with external-field projection operators. *Physical Review A*, *33*(6), 3742. (**DOI:** 10.1103/PhysRevA.33.3742)

[30] Miessler, G.L; Tarr, D. A. Inorganic Chemistry; Pearson-Prentice Hall: Upper Saddle River, NJ, 2004; pp 311-315.

[31] Imbert, C., Hratchian, H., Lanznaster, M., Heeg, M., Hryhorczuk, L., Mcgarvey, B., Verani, C. Influence of Ligand Rigidity and Ring Substitution on the Structural and Electronic Behavior of Trivalent Iron and Gallium Complexes with Asymmetric Tridentate Ligands. *Inorganic Chemistry, 44*, 7414-7422, 2005. (**DOI:** 10.1021/ic050658j)

[32] Gross, K. C., & Seybold, P. G. (2001). Substituent effects on the physical properties and pKa of phenol. *International Journal of Quantum Chemistry*,*85*(4-5), 569-579. (**DOI:** 10.1002/qua.1525)

[33] Liptak, M. D., Gross, K. C., Seybold, P. G., Feldgus, S., & Shields, G. C. (2002). Absolute p K a determinations for substituted phenols. *Journal of the American Chemical Society*, *124*(22), 6421-6427. (**DOI:** 10.1021/ja012474j)

[34] Souza, E. T., Castro, L. C., Castro, F. A. V., do Canto Visentin, L., Pinheiro, C. B., Pereira, M. D., Machado, S. P., Scarpellini, M. (2009). Synthesis, characterization and biological activities of mononuclear Co (III) complexes as potential bioreductively activated prodrugs. *Journal of inorganic biochemistry*, *103*(10), 1355-1365. (**DOI:** 10.1016/j.jinorgbio.2009.07.008)

[35] Wilson, W. R., & Hay, M. P. (2011). Targeting hypoxia in cancer therapy. *Nature Reviews Cancer*, *11*(6), 393-410. (**DOI:** 10.1038/nrc3064)

[36] Ramogida, C. F., Pan, J., Ferreira, C. L., Patrick, B. O., Rebullar, K., Yapp, D. T. T., Lin, Kuo-S., Adam, M. J., Orvig, C. (2015). Nitroimidazole-Containing H_2dedpa and H_2CHXdedpa Derivatives as Potential PET Imaging Agents of Hypoxia with ^{68}Ga. *Inorganic Chemistry, 54,* 4953-4965. (**DOI**: 10.1021/acs.inorgchem.5b00554)

[37] Lanznaster, M., Hratchian, H. P., Heeg, M. J., Hryhorczuk, L. M., McGarvey, B. R., Schlegel, H. B., Verani, C. N. (2006). Structural and Electronic Behavior of Unprecedented Five-Coordinate Iron(III) and Gallium(III) Complexes with a New Phenol-Rich Electroactive Ligand. *Inorganic Chemistry, 45*, 955-957. (**DOI**: 10.1021/ic050809i)

[38] Denny, W. A. (2001). Prodrug strategies in cancer therapy. *European Journal of Medicinal Chemistry*, *36* (7), 577-595. (**DOI:** 10.1016/S0223-5234(01)01253-3)

Tables

Table 1. Crystal data and structure refinement for complexes **C1**–**C4**.

	C1	**C2**	**C3**	**C4**
Empirical formula	$C_{24}H_{22}GaN_9O_9$	$C_{25}H_{28}Br_2ClGaN_6O_8$	$C_{25}H_{26}Cl_3GaN_6O_7$	$C_{27}H_{33}ClGaN_6O_{10}$
Formula weight	650.22	805.52	698.59	706.76
Temperature/K	293(2)	293(2)	293(2)	293(2)
Crystal system	Monoclinic	Monoclinic	Orthorhombic	Monoclinic
Space group	$P2_1/n$	$P2_1/n$	Pbca	Cc
a/Å	8.6545(17)	18.846(4)	16.0687(7)	13.675(3)
b/Å	13.987(3)	18.893(4)	17.3818(9)	14.476(3)
c/Å	21.911(4)	19.287(4)	20.7575(10)	15.612(3)
α/°	90	90	90	90
β/°	95.12(3)	118.65(3)	90	95.95(3)
γ/°	90	90	90	90
Volume/$Å^3$	2641.7(9)	6026(3)	5797.6(5)	3073.7(11)
Z	4	8	8	4
$\rho_{calc}g/cm^3$	1.635	1.776	1.601	1.527
μ/mm^{-1}	1.114	3.712	1.281	1.048
F(000)	1328.0	3216.0	2848.0	1460.0
Crystal size/mm^3	0.276 × 0.2 × 0.109	0.33 × 0.31 × 0.21	0.38 × 0.118 × 0.11	0.42 × 0.16 × 0.09
Radiation	MoKα (λ = 0.71073)	MoKα (λ = 0.71073)	MoKα (λ = 0.71073)	MoKα (λ = 0.71073)
2Θ range for data collection/°	4.734 to 50.694	6.04 to 50.7	3.97 to 52.046	7.546 to 50.698
Index ranges	-10 ≤ h ≤ 10, -16 ≤ k ≤ 16, -26 ≤ l ≤ 26	-22 ≤ h ≤ 22, -22 ≤ k ≤ 22, -23 ≤ l ≤ 22	-19 ≤ h ≤ 15, -21 ≤ k ≤ 21, -25 ≤ l ≤ 25	-16 ≤ h ≤ 16, -15 ≤ k ≤ 17, -18 ≤ l ≤ 18
Reflections collected	53899	32857	68332	8973
Independent reflections	4842 [R_{int} = 0.0564, R_{sigma} = 0,0298]	10875 [R_{int} = 0.0777, R_{sigma} = 0.1006]	5703 [R_{int} = 0.0803, R_{sigma} = 0.0313]	5056 [R_{int} = 0.0631, R_{sigma} = 0.0594]
Data/restraints/parameters	4842/0/388	10875/4/776	5703/12/446	4982/5/421
Goodness-of-fit on F^2	1.174	1.013	1.120	1.067
Final R indexes [I>=2σ (I)]	R_1 = 0.0375, wR_2 = 0.1016	R_1 = 0.0535, wR_2 = 0.1005	R_1 = 0.0554, wR_2 = 0.1318	R_1 = 0.0463, wR_2 = 0.1012
Final R indexes [all data]	R_1 = 0.0583, wR_2 = 0.1115	R_1 = 0.1397, wR_2 = 0.1291	R_1 = 0.0910, wR_2 = 0.1561	R_1 = 0.0678, wR_2 = 0.1249
Largest diff. peak/hole / e $Å^{-3}$	0.40/-0.44	0.81/-1.05	0.77/-0.55	0.54/-0.36

Table 2. Selected bond lengths and angles for complexes **C1**–**C4**.

Atoms			C1	C2 *mol a*	C2 *mol b*	C3	C4
GA1	O1A		1.940(2)	1.941(6)	1.949(6)	1.941(3)	1.931(6)
GA1	O1B		1.949(2)	1.951(4)	1.941(4)	1.934(3)	1.941(6)
GA1	N1A		2.045(3)	2.058(6)	2.058(6)	2.069(4)	2.061(6)
GA1	N1B		2.038(3)	2.050(6)	2.054(6)	2.054(4)	2.082(7)
GA1	N2A		2.071(3)	2.075(6)	2.088(6)	2.081(3)	2.070(7)
GA1	N2B		2.082(2)	2.073(5)	2.044(5)	2.075(4)	2.065(7)
C1A	O1A		1.289(4)	1.31(1)	1.33(1)	1.301(6)	1.340(9)
C1B	O1B		1.308(3)	1.34(1)	1.33(1)	1.314(5)	1.34(1)
N1A	GA1	N2A	91.1(1)	90.3(2)	90.8(2)	91.1(1)	90.4(2)
N1A	GA1	N2B	94.5(1)	92.4(2)	95.7(2)	93.5(2)	93.4(3)
N1B	GA1	N1A	173.3(1)	177.9(2)	173.1(2)	175.2(2)	175.7(3)
N1B	GA1	N2A	93.5(1)	90.7(2)	92.1(2)	91.9(1)	91.3(3)
N1B	GA1	N2B	90.8(1)	89.5(2)	90.6(2)	90.3(2)	90.6(3)
N2A	GA1	N2B	84.5(1)	90.9(2)	89.2(2)	90.0(1)	88.1(3)
O1A	GA1	N1B	85.3(1)	87.6(2)	87.7(2)	86.7(2)	87.1(3)
O1A	GA1	N1A	90.7(1)	91.5(2)	89.6(2)	90.3(2)	91.5(2)
O1A	GA1	N2A	173.9(1)	177.8(2)	178.1(2)	178.6(1)	175.6(2)
O1A	GA1	N2B	89.5(1)	90.4(2)	88.8(2)	90.2(2)	87.9(3)
O1B	GA1	O1A	95.21(9)	90.1(2)	92.4(2)	91.5(1)	91.5(2)
O1B	GA1	N1B	88.93(9)	88.3(2)	87.7(2)	90.1(2)	90.7(3)
O1B	GA1	N1A	86.06(9)	89.8(2)	86.1(2)	86.2(2)	85.3(2)
O1B	GA1	N2A	90.76(9)	88.5(2)	89.6(2)	88.4(1)	92.6(2)
O1B	GA1	N2B	175.23(9)	177.8(2)	177.9(2)	178.4(2)	178.5(3)

Table 3. *Fac/mer* relative energies for each complex in the series, calculated at several approximations. In each case, the most stable structure is taken as possessing zero energy. Comparison can only be done among isomers.

Species	A[a]	B[b]	C[c]	D[d]
mer-**C1**	0.0	0.0	0.0	0.0
fac- **C1**	38.8	36.5	38.3	36.0
mer- **C2**	0.0	0.0	0.0	0.0
fac- **C2**	36.2	34.0	35.3	33.2
mer- **C3**	0.0	0.0	0.0	0.0
fac- **C3**	36.4	34.5	35.5	33.6
mer- **C4**	0.0	0.0	0.0	0.0
fac- **C4**	35.6	32.9	35.2	32.5

[a]relative *fac*/*mer* energy; [b]relative *fac*/*mer* energy with relativistic correction; [c]relative *fac*/*mer* energy with zero point energy correction; [d] relative *fac*/*mer* energy with relativistic and zero point energy corrections.

Table 4. Electronic and redox data for **HL1**–**HL4** and **C1**–**C4.**

	λ_{max}, nm (ε, M^{-1} cm^{-1})	E_{pc} (V *vs* Fc^+/Fc)		E_{pa} (V *vs* Fc^+/Fc)		
		A	**B**	**C**	**D**	**E**
HL1	405 (5632), 350(5382), 255 (10795), 240 (7586)	-1.86	-2.34	-0.81	0.15	0.50
C1	350 (20137), 250 (22151), 225 (21657)	-1.96	-2.45	-0.90	-0.15	0.26
HL2	410 (1271), 325 (3276), 250 (8911), 220 (22239)	-	-2.43	-	0.36	0.74
C2	370 (8538), 265 (17283), 240 (53589), 225 (52452)	-	-2.44	-	-	0.72
HL3	420 (856), 330 (3176), 250 (8458), 225 (33110)	-	-2.32	-0.54	-	0.50
C3	370 (9762), 265 (17487), 240 (55225),230 (64218)	-	-2.41	-	0.29	0.50
HL4	425 (1055), 345 (4480) 225 (99301), 230 (27512)	-2.18	-2.42	-0.67	0.05	0.46
C4	390 (8722), 275 (17399) 245 (37661), 220 (42586)	-	-2.52	-	0.43	0.80

Table 5: Anti-cancer activity of complex **C1–C4** compared to ligands, $Ga(NO_3)_3•6H_2O$ and the clinically standard drug cisplatin expressed as IC_{50} values.

Compound	IC_{50} (μM)		
	MCF-7	**PC-3**	**A-549**
C1	>200μM	>200μM	94.12 ± 4.62
C2	>200μM	>200μM	> 200
C3	>200μM	>200μM	> 200
C4	>200μM	>200μM	174.70 ± 8.41
HL1	>200μM	>200μM	> 200
HL2	>200μM	>200μM	> 200
HL3	>200μM	>200μM	> 200
HL4	>200μM	>200μM	> 200
$Ga(NO_3)_3•6H_2O$	>200μM	>200μM	> 200
Cisplatin	117.4 ± 6.9	>200μM	135.10 ± 6.5

List of Figure Captions

Figure 1. Schematic view of gallium maltolate (a), KP46 (b), and complexes **C1**–**C4**.

Figure 2. Thermal ellipsoid plot for complex **C1** (top) and perspective view of hydrogen bonds (botton). Ellipsoids at 40% probability level. Counter ion molecules are omitted for clarity.

Figure 3. Electronic spectra of complexes **C1**–**C4** in methanol solution. C = 1.0 $\times 10^{-5}$ mol L^{-1}.

Figure 4. Cytotoxic effect of ligands **HL1**–**HL4**, complexes **C1**–**C4**, $Ga(NO_3)_3 \cdot 6H_2O$ and cisplatin on human cancer cells lines MCF-7 (A and D), PC-3 (B and E) and A-549 (C and F) evaluated by the MTT assay. Results are mean ± SD of three independent experiments.

List of Figures

Figure 1

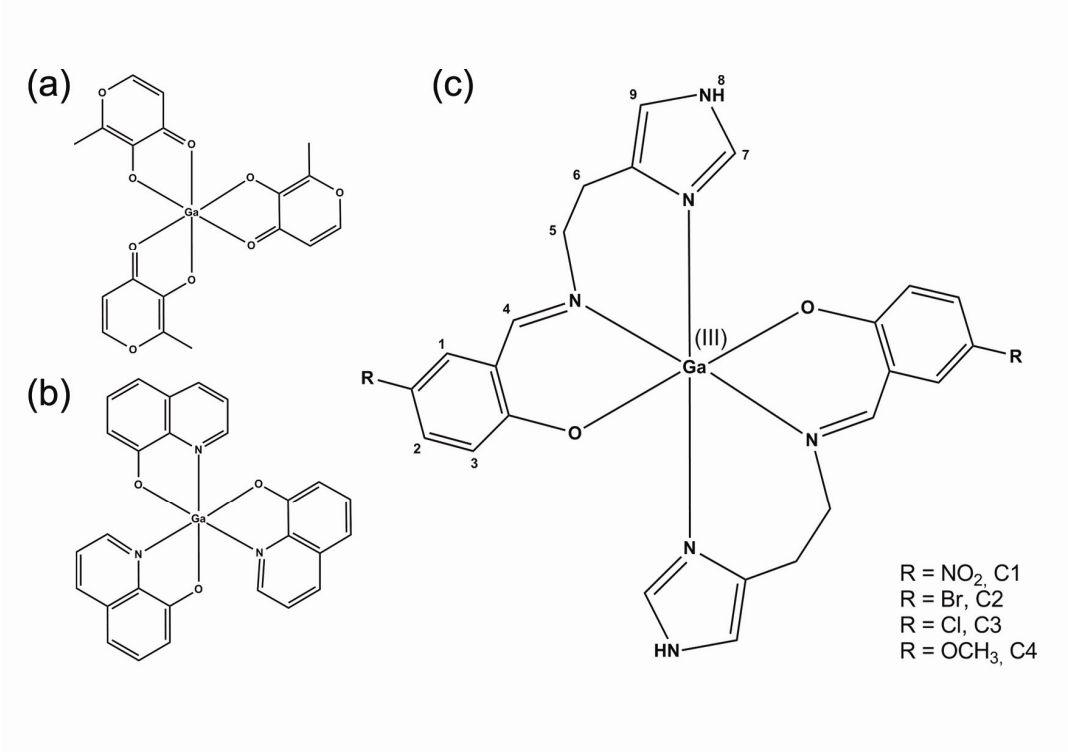

Figure 2

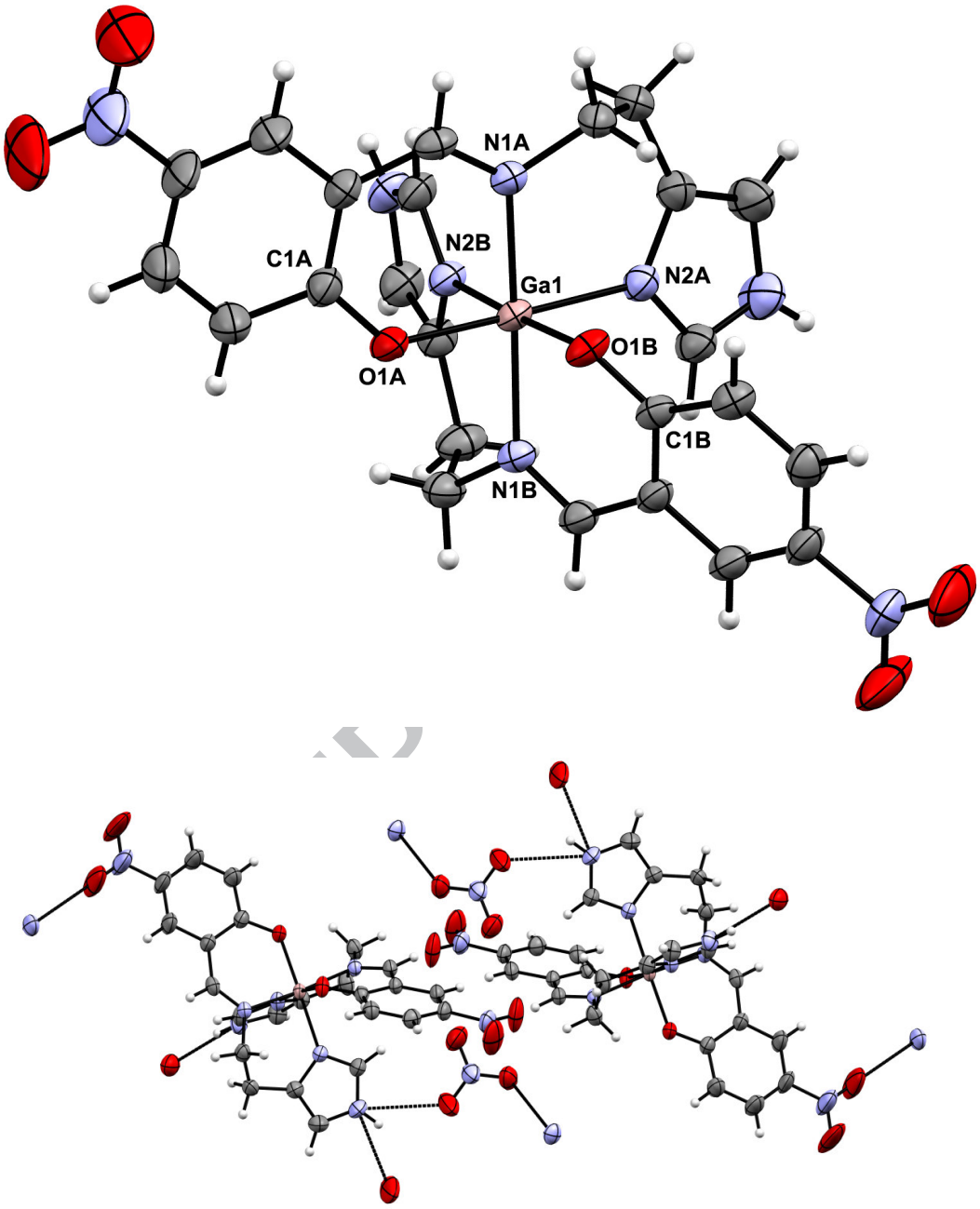

Figure 3

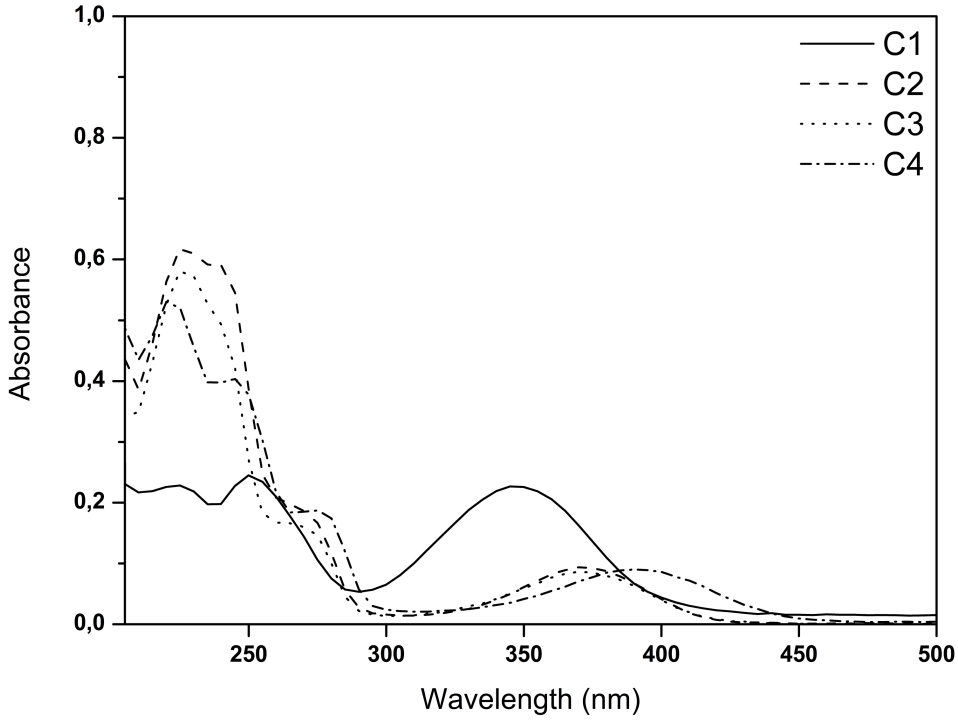

Figure 4

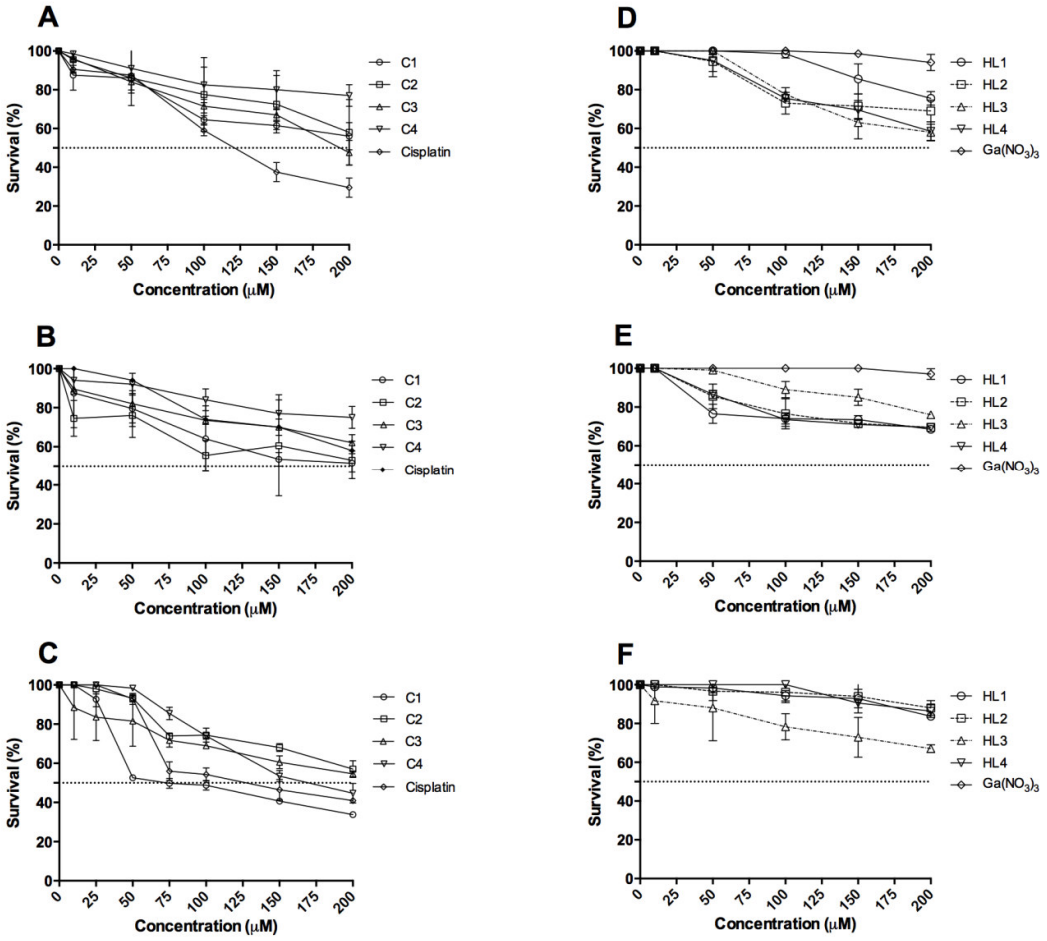

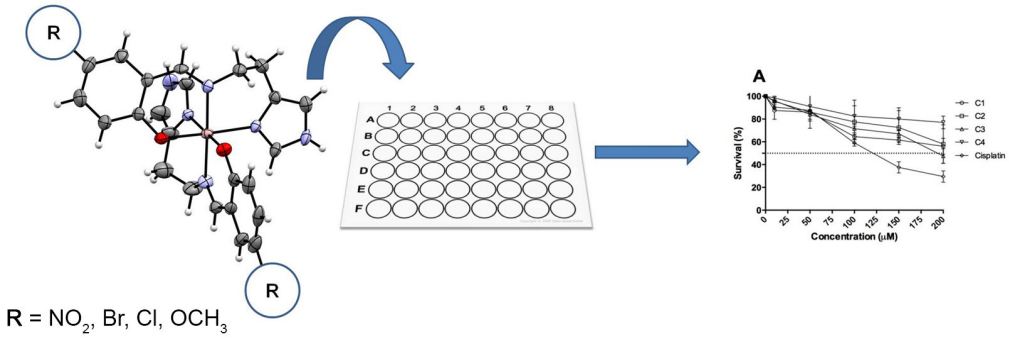

R = NO_2, Br, Cl, OCH_3

Graphical abstract (Synopsis)

Four new mononuclear gallium(III) complexes were synthesized, fully characterized and evaluated against the human tumor cell lines MCF-7, A-549 and PC-3. Complex C1(-NO_2) was the most active, being effective and selective against A-549, with IC_{50} (94.12 ± 4.62) lower than cisplatin (135.10 ± 6.50), which was tested as a metallodrug reference under the same experimental conditions.